Age-related decrements cortical gyrification:

Evidence from an accelerated longitudinal dataset

Christopher R. Madan

School of Psychology, University of Nottingham, Nottingham, UK

† Corresponding author.

Christopher R. Madan
School of Psychology, University Park
University of Nottingham
Nottingham, NG7 2RD, UK.
Email: christopher.madan@nottingham.ac.uk.

Abstract

Cortical gyrification has been found to decrease due to aging, but thus far this has only been examined in cross-sectional samples. Interestingly the topography of these age-related differences in gyrification follow a distinct gradient along the cortex relative to age effects on cortical thickness, likely suggesting a different underlying neurobiological mechanism. Here I examined several aspects of gyrification in an accelerated longitudinal dataset of 280 healthy adults aged 45-92 with an interval between first and last MRI session of up to 10 years (total of 815 MRI sessions). Results suggest that the well-known age changes in sulcal morphology—the enlarging of sulci with age—underlies these changes in gyrification.

Keywords: structural MRI; cortical folding; brain morphology; sulcal morphology

Introduction

In the last decade, brain imaging studies have demonstrated several gradients in activation related to functional networks of regions (e.g., Margulies et al., 2016; Murphy et al., 2019; Sormaz et al., 2018). Distinct cortical gradients in structural properties of the brain also exist, such as in cortical thickness (e.g., Hogstrom et al., 2013; Madan & Kensinger, 2018; Salat et al., 2004; Sowell et al., 2003) and myelination (e.g., Glasser & Van Essen, 2011; Grydekand et al., 2013; Mangeat et al., 2015; Shafee et al., 2015). However, one of the most identifiable characteristics of the human brain is its folding structure. Despite macro-scale consistencies between individuals, everyone's cortical folding pattern is unique. These folding patterns do change however due to aging, though the underlying process of this change that is not well understood. Here I examined gyrification in an accelerated longitudinal dataset to obtain further insight into these age changes, as well as examine the topography of gyrification and how gyrification relates to other measures of cortical folding.

Elias and Schwartz (1969) developed a procedure to quantify cortical gyrification as a ratio between the area of the total cortical surface relative to the ‘exposed’ surface. Given limitations of contemporary technologies, a stereological approach, and was later refined to be based on lengths of pial and outer contour lengths estimated from coronal sections by Zilles et al. (1988). Extending this procedure, Schaer et al. (2008, 2012) developed an automated approach for calculating cortical gyrification from a surface mesh, through the generation of an outer surface that encloses the gray matter surface generated by FreeSurfer.

As initially shown by Zilles et al. (1988) and replicated in more recent studies (e.g., Hogstrom et al., 2013; Madan & Kensinger, 2016), gyrification is most pronounced in the parietal and temporal lobes. Several studies have shown that global cortical gyrification decreases with age in several cross-sectional samples (Cao et al., 2017; Hogstrom et al., 2013; Lamballais et al., 2020; Madan & Kensinger, 2016, 2018; Madan, 2018). Moreover, it

has also been shown that the topography of these changes is distinct from cortical thickness, where gyrification primarily decreases in the parietal lobe (e.g., Hogstrom et al., 2013; Madan & Kensinger, 2016, 2018). Cortical thickness, in contrast, primarily decreases in frontal and temporal regions—with age decreases associated with decreases in dendritic density of pyramidal neurons as well as changes in cortical myelination affecting gray/white matter contrast, mechanisms distinct from age changes in gyrification. Further demonstrating the utility of gyrification measurements, studies of patient populations have demonstrated differences in gyrification relative to healthy individuals in relation to Alzheimer's disorder (King et al., 2010; Liu et al., 2012), schizophrenia (Cao et al., 2017; Palaniyappan & Liddle, 2012; Palaniyappan et al., 2015), autism (Schaer et al., 2013), and major depression disorder (Cao et al., 2017), among other psychiatric disorders.

Based on with prior investigations of global gyrification—it has previously been estimated in cross-sectional data to decrease by approximately 0.035 GI/decade (Madan & Kensinger, 2016; Madan, 2018), however, there is also consideration of measurement reliability, (e.g., mean within-subjects deviation of 0.04 in Madan & Kensinger [2017] in a dataset where sessions were merely days apart, used to assess test-retest reliability). Moreover, when cross-sectional data has been plotted, there is a large amount of off-axis variability (i.e., age-unrelated) indicating that, though reproducible, the coupling between gyrification and aging is relatively weak and influenced by many other factors. Based on these considerations, a longitudinal dataset with larger interval between scans would be prudent for evaluating the influence of aging on cortical gyrification.

Here I examine changes in cortical gyrification in an accelerated longitudinal sample to more directly examine how cortical folding can change within age on the individual level, rather than in cohorts/cross-sectional datasets. While accelerated longitudinal samples have been used previously to examine age changes in other morphological measures such as

cortical thickness (e.g., Storsve et al., 2014), this has yet to be done with gyrification. It is currently not clear how gyrification changes with aging—for instance, is the decrease in gyrification in the parietal lobe more evident because the parietal lobe has the highest gyrification? Alternatively, does the distribution of gyrification change with age?

Methods

Dataset

Data from 280 healthy adults (aged 45-92) from the OASIS-3 (Open Access Series of Imaging Studies 3) dataset (LaMontagne et al., 2019) were included in the analyses presented here. From the full dataset, participants were only included in the present analyses if four conditions were met. (1) There must be at least two MRI sessions available with T1 volumes collected. (2) MRI data had to be collected using either the Siemens TIM Trio 3 T scanner or Siemens BioGraph mMR PET-MR 3 T scanner (less than 5% of the otherwise available data were collected using one of three other MRI scanners). (3) There had to be an interval from first to last MRI session spanning at least three years. (4) From the clinical sessions, there had a Clinical Dementia Rating (CDR) score of zero at every assessment. All raw data is available from https://www.oasis-brains.org.

Across the 280 included adults, the Mini-Mental State Exam (MMSE) was administered in a total of 1904 clinical sessions, with between 2 and 20 clinical sessions per participant ($M \pm SD$ = 6.70±3.21 administrations). Of the 1904 administrations, only four yielded an MMSE score below 25. For two individuals these sub-25 MMSE scores were later followed by higher MMSE scores (here, scoring at least 29) on multiple subsequent administrations. For the remaining two individuals, these were the last MMSE scores recorded (for these specific individuals, there were 5 and 9 MMSE administrations, respectively).

The interval between the first and last MRI session acquired for each participant ranged from 3 to 10 years (*M*±*SD* = 5.47±1.91 years). Of the 280 participants, 117 had two MRI sessions, 96 had three sessions, 45 had four sessions, and 22 had five or more sessions (to a maximum of seven). In total, 1138 T1 volumes from 815 MRI sessions were examined. If more than one T1 scan was acquired during an MRI session, all volumes were processed (see procedure below) and the gyrification estimates for the scans was averaged (same for other T1-derived measures).

Structural data was collected using two different Siemens 3 T MRI scanners with MPRAGE sequences: (1) 586 of the 820 MRI sessions were collected with a Siemens TIM Trio 3 T scanner, with parameters: TR=2.4 ms; TE=3.2 ms; flip angle=8°; voxel size=1×1×1 mm. (2) The remaining 234 MRI sessions were collected with a Siemens BioGraph mMR PET-MR 3 T scanner, with parameters: TR=2.3 ms; TE=3.0 ms; flip angle=9°; voxel size=1×1×1 mm.

MRI Processing

All T1 volumes were processed using FreeSurfer v6.0 on a machine running RedHat 4.8.5-16 (Fischl, 2012; Fischl & Dale, 2000; Fischl et al., 2002). (Note, these are not the same FreeSurfer outputs as publicly distributed from OASIS, which were estimated using older versions of FreeSurfer.) All T1 volumes were processed independently with the standard FreeSurfer pipeline (i.e., `recon-all`), i.e., not using the longitudinal processing pipeline, to allow the individual scan derived measures to be comparable in reliability to previous cross-sectional studies. Gyrification was calculated using FreeSurfer, as described in Schaer et al. (2008, 2012), and is illustrated in Figure 1.

Sulcal morphology (width and depth) was also estimated for 16 major sulci, using the calcSulc toolbox (Madan, 2019a). The sulci are the central, post-central, superior frontal,

inferior frontal, parieto-occipital, occipito-temporal, middle occipital and lunate, and marginal part of the cingulate sulci, in both the left and right hemispheres. Analyses here are only conducted on the mean sulcal width and depth, averaging across the 16 sulci.

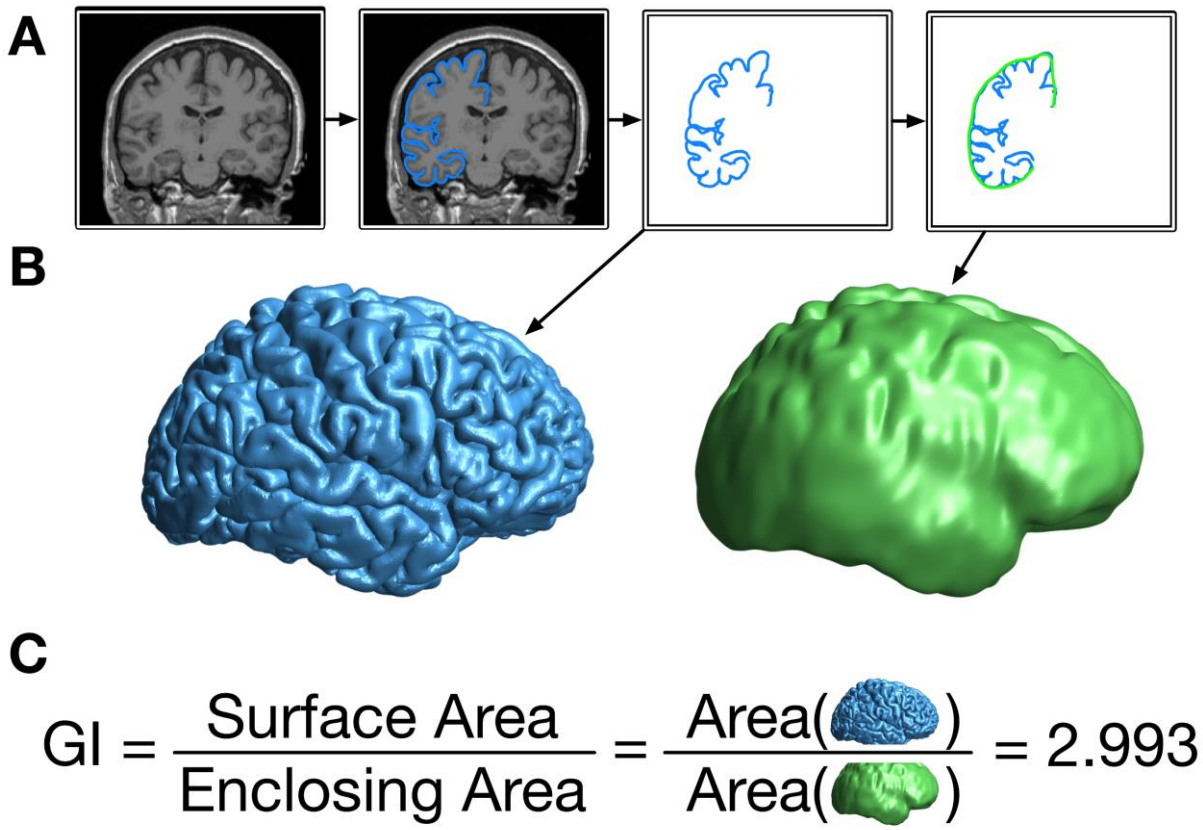

Figure 1. Illustration of the calculation procedure for global gyrification. (A) From the original T1 volume, the outer contour of the gray matter is traced, and then surrounded by a smooth enclosing surface. (B) When done as a 3D surface, this results in the pial (blue) and enclosing (green) surfaces. (C) The gyrification index (GI) is the ratio of the cortical surface area divided by the surface area of the enclosing surface.

Anterior-posterior gradient in gyrification. Gyrification measurements for each MRI session were resampled to the common surface space using FreeSurfer's spherical surface co-registration (Fischl et al., 1999). This common surface space was then divided into 200 coronal sections, analogous to the contour procedure used by Zilles et al. (1988). This allows for mean gyrification to be simplified into an anterior-posterior plot. Note that, however, vertex-wise gyrification measures were first estimated based on the Schaer et al. (2012)

procedure that relies on 25 mm radius local region of interest, gyrification values for each section are spatially autocorrelated with adjacent sections. To-date there do not appear to be any publications that have examined the anterior-posterior gyrification pattern using the FreeSurfer gyrification calculation implementation (i.e., the Schaer et al. [2012] approach).

Results

Global gyrification

Before examining the topography of gyrification, it seemed sensible to evaluate age changes in global gyrification, which itself has not been examined yet in a longitudinal dataset. The decline in gyrification was estimated using a linear mixed effects model to estimate the slope (allowing for random y-intercept for each participant). As shown in Figure 2, the age fixed effect was statistically significant [$t(813)=14.41$, $p<.001$] with a decreasing slope of 0.04291 GI/decade [95% C.I. = 0.03499—0.04603]. While studies examining cross-sectional data suggest that gyrification involves a large degree of age-independent variability, the longitudinal data plotted here clearly show a relatively consistent age decline, distinct from differences in the y-intercept of the gyrification index.

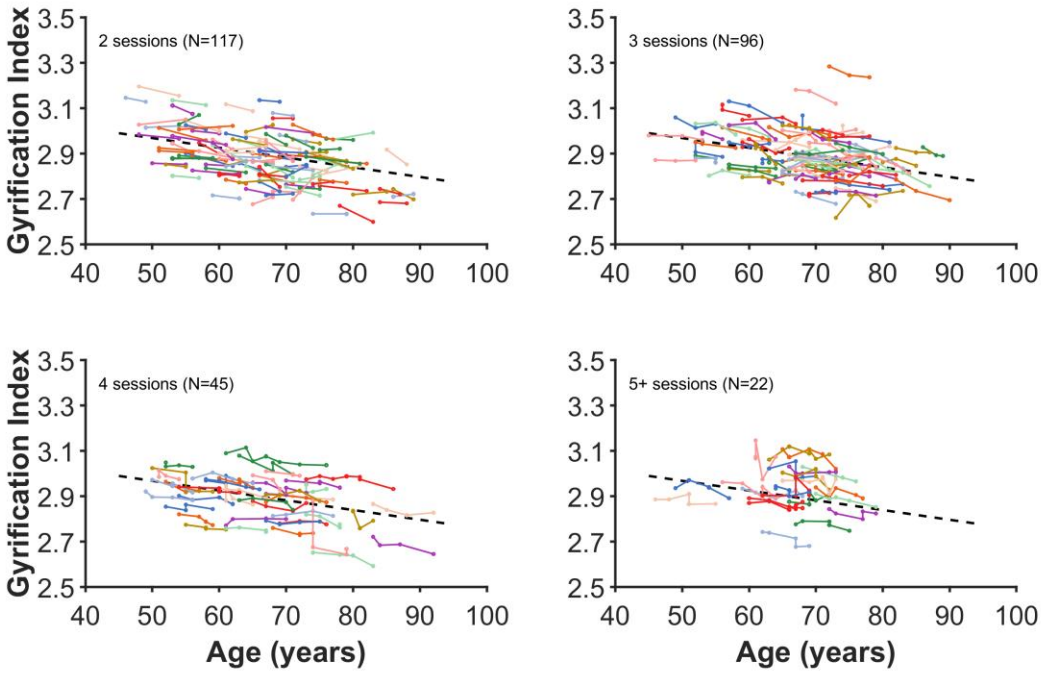

Figure 2. Age changes in global gyrification. Each coloured line represents an individual participant, with each dot corresponding to an MRI session. The plot has been divided into panels for each set of timepoints to improve readability. Dashed line present in all panels shows the decrease in global gyrification based on all data, estimated using the linear mixed effects model.

Anterior-posterior gradient in gyrification

The results of this analysis are shown in Figure 3. While aging has not previously been investigated using this approach, the overall gradient (i.e., the upper row) is relatively consistent with Zilles et al. (1988, Fig. 6). As in Zilles, looking from anterior to posterior, the gradient gradually rises to a peak mid-way through the frontal lobe (approx. percentile 75), followed by a relative plateau through the section that subtends the temporal lobe, with a trough as the anterior-posterior section is increasingly represented by the parietal lobe (percentile 37). A higher plateau peak subtends the parietal lobe, and then gradually declines as gradient transitions into the occipital lobe (beginning from around percentile 15).

The middle and lower rows of Figure 3 show that while gyrification decreases globally, they are most pronounced in the parietal lobe. Further examinations of the surface topography can be used to further differentiate gyrification in parietal and temporal regions.

These aging results clearly demonstrate that the overall distribution of gyrification does not change with age, it merely diminishes in magnitude.

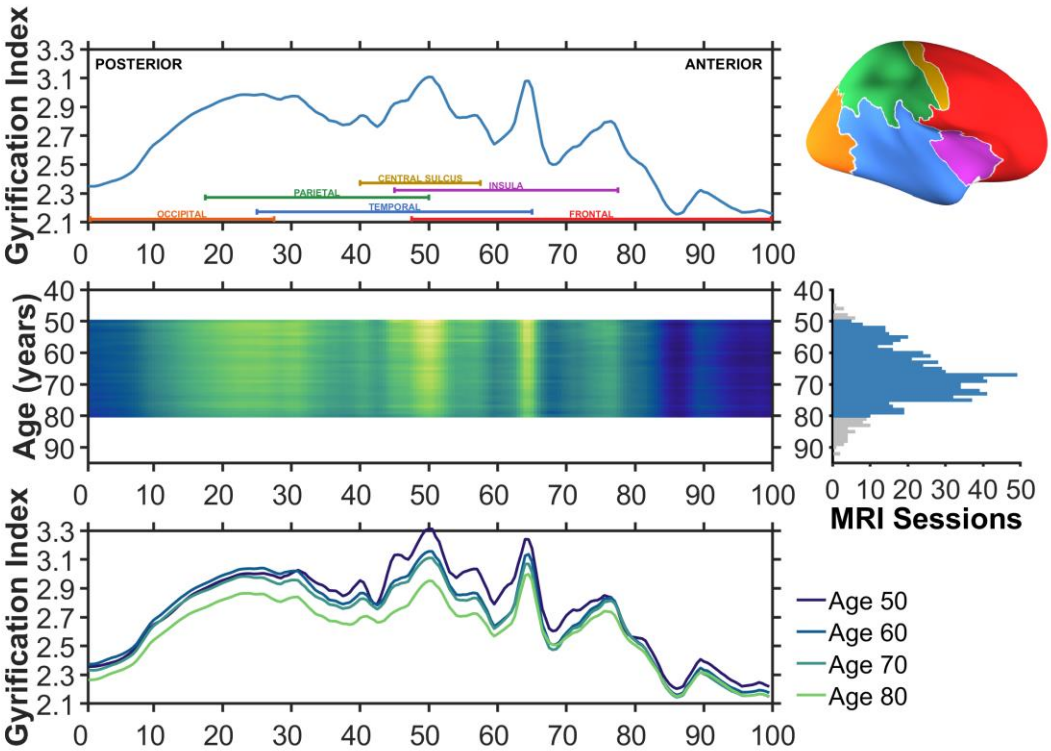

Figure 3. Gyrification index across posterior (percentile 0; caudal) to anterior (percentile 100; rostral). The upper row illustrates the average gyrification across the common surface space. Coloured labels denoting each of the four lobes (frontal: red; parietal: green; temporal: blue; occipital: orange), insula (purple), and central sulcus (yellow) are included to aid in interpretation. An inflated cortical surface is shown on the right to help visualise the relative extents of these regions, though a folded brain was used for the actual analyses. The middle row shows the mean anterior-posterior gyrification for each age between 50 and 80, inclusive; brighter colours denote regions of higher gyrification index. This subset of ages was selected based on having sufficient sessions per age to use in the estimation, as shown in the right panel. A total of 746 of the available 815 MRI sessions were in this age range. The lower row shows the mean anterior-posterior gyrification for individuals aged 50, 60, 70, and 80. Aging is associated with overall decreases in gyrification, but these appear to be most pronounced in the parietal lobe.

Topography of gyrification

As gyrification is calculated as the ratio of areas of the cortical surface to an enclosing surface, the gyrification index is highest at the insula—as shown Figure 4A (and previously shown by Schaer et al., 2008; Cao et al., 2017; Lamballais et al., 2020; and others). As aforementioned, previous studies have demonstrated age differences in gyrification, but only in cross-sectional samples (Cao et al., 2017; Hogstrom et al., 2013; Lamballais et al., 2020; Madan & Kensinger, 2016, 2018; Madan, 2018). Here I found a similar pattern in the present accelerated longitudinal dataset, as shown in Figure 4B. The decline in gyrification is most pronounced in the parietal lobe and posterior aspects of the frontal lobe. However, on individual cortical surfaces, even examining changes over nearly a decade, changes in the surfaces are only barely visible (see Figure 5).

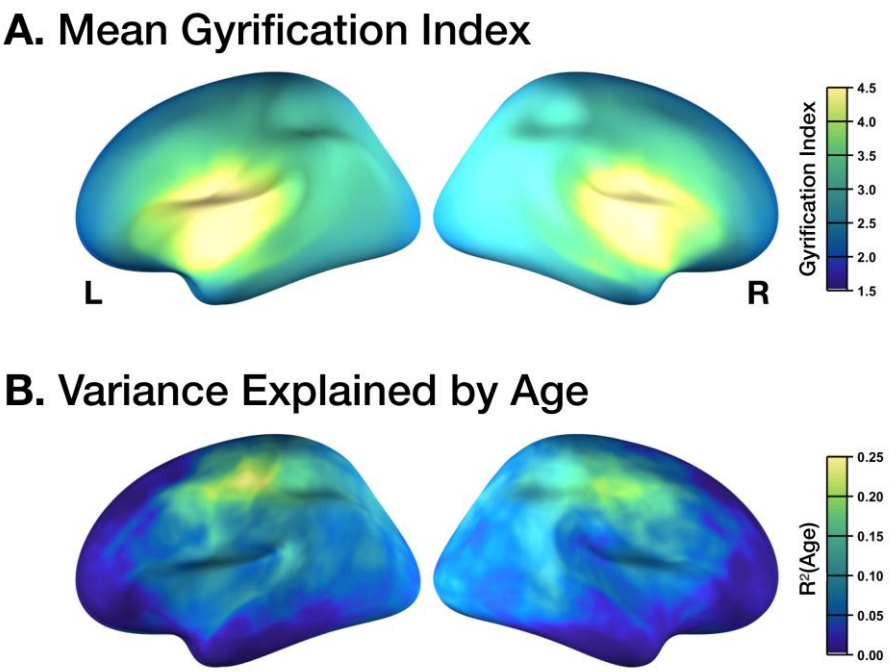

Figure 4. Topography of gyrification. (A) Mean gyrification, with the highest values corresponding to the insula. (B) Age changes in gyrification, with the highest values corresponding to the parietal lobe and posterior aspects of the frontal lobe.

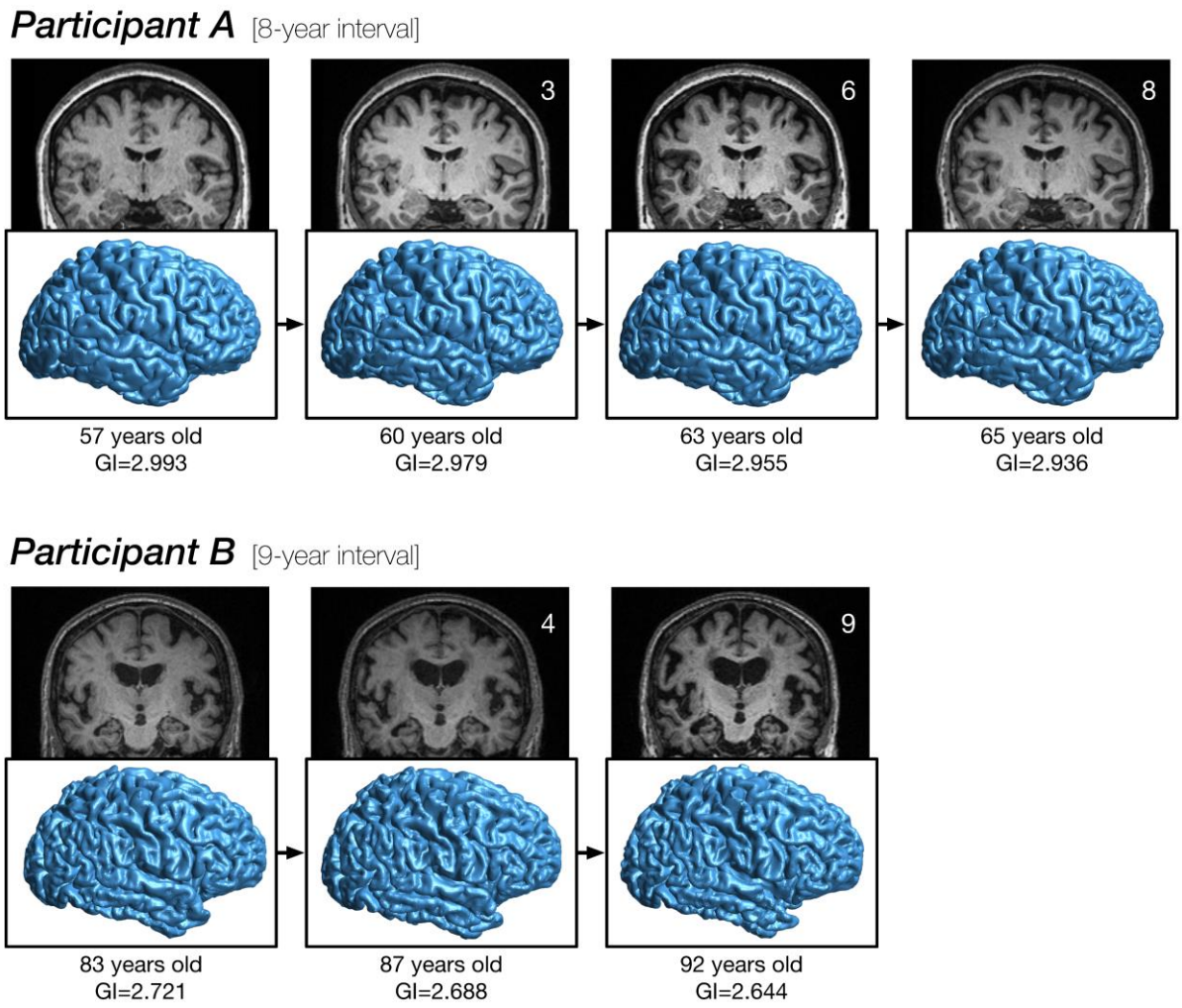

Figure 5. Longitudinal age changes in cortical folding. Cortical surface reconstructions for two participants, illustrating changes in folding over nearly a decade each. GI denotes gyrification index. See Madan (2015) for details related to rendering the cortical surfaces.

Sulcal prominence

Figure 5 shows that the overall pattern of cortical folding remains relatively consistent, despite consistent, though small, decreases in the gyrification index. Looking at the MRIs themselves, however, does indicate changes in the sulcal width and depth, readily apparent by visual inspection. Here I examined how well global measures of sulcal morphology, both width and depth, can alternatively explain variability in gyrification.

To test this, I conducted a hierarchical linear mixed effect analysis with four models. In each case the dependent variable was the gyrification index. The first three models

included a fixed effect of either age, sulcal width, or sulcal depth, and included a random intercept. The first model is the same linear mixed effects model as reported earlier in the global gyrification section. The fourth model included all three predictors. The results of this analysis are reported in Table 1.

Model	Linear Mixed Effects Equation	*ΔBIC*	Fixed Effect	*t*
1	GI ~ Age + (1|Subject)	302.45	Age	14.41
2	GI ~ SulcalWidth + (1|Subject)	473.19	SulcalWidth	3.69
3	GI ~ SulcalDepth + (1|Subject)	20.35	SulcalDepth	25.12
4	GI ~ Age + SulcalWidth + SulcalDepth + (1|Subject)	0.00	Age	5.41
			SulcalWidth	0.88
			SulcalDepth	19.28

Table 1. Heirarchical linear mixed effects model of global gyrification index with age, sulcal width, and sulcal depth. All fixed effects were significant (all *p*s<.05); the degrees of freedom for models 1-3 is 813, and for model 4 is 811.

Model 4 explains the data better than models 1-3. Nonetheless, of the first three models, the sulcal depth model outperforms the other two models by a large margin. Taken together this indicates that sulcal depth is the single most related measure here, moreso than age, in explaining variations in gyrification index, though age can still contribute unique variance that is independent of sulcal depth and width.

Providing further support, a model with sulcal width as the dependent variable with only age (and random intercepts) as predictors resulted in a stronger effect of age [$t(813)=16.41$, $p<.001$].

Discussion

From the global gyrification and anterior-posterior analyses, it is clear that the age decreases in gyrification are gradual. Moreover, the anterior-posterior analysis was designed to evaluate if these age changes in gyrification were related to a shifts in the underlying distribution of

cortical folding, but this does not appear to be the case. Instead, there is a global decrease, with some regions more affected, as highlighted in the topography analyses. Converging with prior cross-sectional studies, these regions most affected in gyrification with age are distinct from those affected in cortical thickness.

Despite the numerous prior studies previously reporting decreases in gyrification with age, the results and discussion of these studies provide little towards explaining the underlying mechanism. Many prior studies of brain morphology have indicated that cortical surface area is not affected by aging (e.g., McKay et al., 2014; Storsve et al., 2014). This age consistency also rules out any systematic changes in the minor deformations in the folds along the gyri that would be measured by indicies of the spatial frequency/power spectra of cortical folding as providing information distinct from gyrification itself (as in Madan, 2019b). However, long before neuroimagers began to examine cortical thickness as an index of cortical atrophy, radiologists have qualitatively assessed sulcal prominence—alternatively referred to as widening, enlargement, or dilation—as a key measure of age-related atrophy (Coffey et al., 1992; Drayer, 1988; Huckman et al., 1975; Jacoby et al., 1980; Laffey et al., 1984; LeMay, 1984; Pasquier et al., 1996; Roberts & Caird, 1976; Scheltens et al., 1997; Tomlinson et al., 1968; Turkheimer et al., 1984; Yue et al., 1997). Indeed, by visual inspection, cortical atrophy is much more readily assessed from sulcal features than from cortical thickness (see Figure 5).

Using current automated methods, sulcal morphology can also be quantitatively measured, where the width and depth of major sulci can be identified and estimated (e.g., Kochunov et al., 2005; Madan, 2019a). Across a number of studies and samples (albeit generally with much smaller samples), sulcal morphology has been reliably associated with age-related differences (Jin et al., 2018; Kochunov et al., 2005; Li et al., 2011; Liu et al., 2010, 2013; Madan, 2019a; Rettmann et al., 2006; Shen et al., 2018). The work presented is

able to provide additional specificity in how gyrification appears to decrease with age, a step towards understanding the underlying mechanism: Here I show that gyrification changes can be considered as being strongly related to changes in the underlying sulcal morphology, particularly depth. However, despite this well-established relationship between sulcal morphology and aging, the neurobiological mechanism underlying this change in the fundamental organisation of cortical folding yet remains unclear and remains a topic for further study.

More generally, this work adds to the growing literature demonstrating that the availability of open-access MRI data can facilitate advances in our understanding of brain morphology well beyond the goals of the researchers originally collecting the data (see Madan, 2017, for an overview of benefits and considerations). It is worth acknowledging that the results presented here likely underestimate the extent that gyrification decreases with age. Older adults that are interested and able to participate in a research study in their 80s and 90s are very likely to be a biased sample of individuals for their age cohort, demonstrating greater physical and mental health than many of their peers (i.e., an issue of external validity; see Pearl & Bareinboim, 2014, and Keyes & Westreich, 2019, for more nuanced discussions).

Acknowledgments

This work would not have been possible without data from OASIS-3 and the funding that supported it (Principal Investigators: T. Benzinger, D. Marcus, J. Morris; NIH P50AG00561, P30NS09857781, P01AG026276, P01AG003991, R01AG043434, UL1TR000448, R01EB009352). I would also like to acknowledge the support of NVIDIA Corporation with the donation of a Titan Xp GPU that was used in this research.

References

Cao, B., Mwangi, B., Passos, I.C., Wu, M.-J., Keser, Z., Zunta-Soares, G.B., Xu, D., Hasan, K.M. & Soares, J.C. (2017). Lifespan gyrification trajectories of human brain in healthy individuals and patients with major psychiatric disorders. *Scientific Reports, 7,* 511. doi:10.1038/s41598-017-00582-1

Coffey, C. E., Wilkinson, W. E., Parashos, L., Soady, S., Sullivan, R. J., Patterson, L. J., ... Djang, W. T. (1992). Quantitative cerebral anatomy of the aging human brain: A cross-sectional study using magnetic resonance imaging. *Neurology, 42,* 527–527. doi:10.1212/wnl.42.3.527372

Drayer, B. P. (1988). Imaging of the aging brain. Part I. normal findings. Radiology, 166, 785–796. doi: 10.1148/radiology.166.3.3277247

Elias, H., & Schwartz, D. (1969). Surface areas of the cerebral cortex of mammals determined by sterological methods. *Science, 166*(3901), 111-113. doi:10.1126/science.166.3901.111

Fischl, B. (2012). FreeSurfer. *NeuroImage, 62,* 774–781. doi:10.1016/j.neuroimage.2012.01.021

Fischl, B., & Dale, A. M. (2000). Measuring the thickness of the human cerebral cortex from magnetic resonance images. *Proceedings of the National Academy of Sciences, 97,* 11050–11055. doi:10.1073/pnas.200033797

Fischl, B., Salat, D. H., Busa, E., Albert, M., Dieterich, M., Haselgrove, C., … Dale, A. M. (2002). Whole brain segmentation: Automated labeling of neuroanatomical structures in the human brain. *Neuron, 33,* 341–355. doi:10.1016/s0896-6273(02)00569-x

Fischl, B., Sereno, M. I., Tootell, R. B. H., & Dale, A. M. (1999). High-resolution intersubject averaging and a coordinate system for the cortical surface. *Human Brain Mapping, 8(4),* 272–284. doi:10.1002/(sici)1097-0193(1999)8:4<272::aid-hbm10>3.0.co;2-4

Glasser, M. F., & Van Essen, D. C. (2011). Mapping human cortical areas in vivo based on myelin content as revealed by T1- and T2-weighted MRI. *Journal of Neuroscience, 31(32),* 11597–11616. doi:10.1523/jneurosci.2180-11.2011

Grydeland, H., Walhovd, K. B., Tamnes, C. K., Westlye, L. T., & Fjell, A. M. (2013). Intracortical myelin links with performance variability across the human lifespan: Results from T1- and T2-weighted MRI myelin mapping and diffusion tensor imaging. *Journal of Neuroscience, 33(47),* 18618–18630. doi:10.1523/jneurosci.2811-13.2013

Hogstrom, L.J., Westlye, L.T., Walhovd, K.B. & Fjell, A.M. (2013). The structure of the cerebral cortex across adult life: Age-related patterns of surface area, thickness, and gyrification. *Cerebral Cortex, 23,* 2521–2530. doi:10.1093/cercor/bhs231

Huckman, M. S., Fox, J., & Topel, J. (1975). The validity of criteria for the evaluation of cerebral atrophy by computed tomography. *Radiology, 116(1),* 85–92. doi:10.1148/116.1.85

Jin, K., Zhang, T., Shaw, M., Sachdev, P., & Cherbuin, N. (2018). Relationship between sulcal characteristics and brain aging. *Frontiers in Aging Neuroscience, 10,* 339. doi:10.3389/fnagi.2018.00339

Keyes, K. M., & Westreich, D. (2019). UK Biobank, big data, and the consequences of non-representativeness. *The Lancet, 393(10178),* 1297. doi:10.1016/s0140-6736(18)33067-8

King, R. D., Brown, B., Hwang, M., Jeon, T., & George, A. T. (2010). Fractal dimension analysis of the cortical ribbon in mild Alzheimer's disease. *NeuroImage, 53,* 471–479. doi:10.1016/j.neuroimage.2010.06.050

Laffey, P. A., Peyster, R. G., Nathan, R., Haskin, M. E., & McGinley, J. A. (1984). Computed tomography and aging: Results in a normal elderly population. *Neuroradiology, 26,* 273–278. doi: 10.1007/BF00339770

Lamballais, S., Vinke, E. J., Vernooij, M. W., Ikram, M. A., & Muetzel, R. L. (2020). Cortical gyrification in relation to age and cognition in older adults. *NeuroImage*, 116637. doi:10.1016/j.neuroimage.2020.116637

LaMontagne, P. J., Benzinger, T. L. S., Morris, J. C., Keefe, S., Hornbeck, R., Xiong, C., … Marcus, D. (2019). OASIS-3: Longitudinal neuroimaging, clinical, and cognitive dataset for normal aging and Alzheimer's disease. *medRxiv*. doi:10.1101/2019.12.13.19014902

LeMay, M. (1984). Radiologic changes of the aging brain and skull. *American Journal of Roentgenology, 143(2)*, 383–389. doi:10.2214/ajr.143.2.383

Li, S., Xia, M., Pu, F., Li, D., Fan, Y., Niu, H., … He, Y. (2011). Age-related changes in the surface morphology of the central sulcus. *NeuroImage, 58(2)*, 381–390. doi:10.1016/j.neuroimage.2011.06.041

Liu, T., Lipnicki, D. M., Zhu, W., Tao, D., Zhang, C., Cui, Y., Jin, J. S., Sachdev, P. S., & Wen, W. (2012). Cortical gyrification and sulcal spans in early stage Alzheimer's disease. *PLOS ONE, 7(2)*, e31083. doi:10.1371/journal.pone.0031083

Liu, T., Sachdev, P. S., Lipnicki, D. M., Jiang, J., Geng, G., Zhu, W., Reppermund, S., Tao, D., Trollor, J. N., Brodaty, H., & Wen, W. (2013). Limited relationships between two-year changes in sulcal morphology and other common neuroimaging indices in the elderly. *NeuroImage, 83*, 12–17. doi:10.1016/j.neuroimage.2013.06.058

Liu, T., Wen, W., Zhu, W., Trollor, J., Reppermund, S., Crawford, J., Jin, J. S., Luo, S., Brodaty, H., & Sachdev, P. (2010). The effects of age and sex on cortical sulci in the elderly. *NeuroImage, 51(1)*, 19–27. doi:10.1016/j.neuroimage.2010.02.016

Madan, C. R. (2015). Creating 3D visualizations of MRI data: A brief guide. *F1000Research, 4*, 466. doi:10.12688/f1000research.6838.1

Madan, C. R. (2017). Advances in studying brain morphology: The benefits of open-access data. *Frontiers in Human Neuroscience, 11*, 405. doi:10.3389/fnhum.2017.00405

Madan, C. R. (2018). Age differences in head motion and estimates of cortical morphology. *PeerJ, 6*, e5176. doi:10.7717/peerj.5176

Madan, C. R. (2019a). Robust estimation of sulcal morphology. *Brain Informatics, 6*, 5. doi:10.1186/s40708-019-0098-1

Madan, C. R. (2019b). Evaluating the angular power spectrum of cortical folding. *Proceedings of the Cognitive Computational Neuroscience Annual Meeting, 3*, 496-499. doi:10.32470/CCN.2019.1177-0

Madan, C. R., & Kensinger, E. A. (2016). Cortical complexity as a measure of age-related brain atrophy. *NeuroImage, 134*, 617-629. doi:10.1016/j.neuroimage.2016.04.029

Madan, C. R., & Kensinger, E. A. (2017). Test-retest reliability of brain morphology estimates. *Brain Informatics, 4*, 107-121. doi:10.1007/s40708-016-0060-4

Madan, C. R., & Kensinger, E. A. (2018). Predicting age from cortical structure across the lifespan. *European Journal of Neuroscience, 47*, 399-416. doi:10.1111/ejn.13835

Mangeat, G., Govindarajan, S. T., Mainero, C., & Cohen-Adad, J. (2015). Multivariate combination of magnetization transfer, T2* and B0 orientation to study the myelo-architecture of the in vivo human cortex. *NeuroImage, 119*, 89–102. doi:10.1016/j.neuroimage.2015.06.033

Margulies, D. S., Ghosh, S. S., Goulas, A., Falkiewicz, M., Huntenburg, J. M., Langs, G., Bezgin, G., Eickhoff, S. B., Castellanos, F. X., Petrides, M., Jefferies, E., & Smallwood, J. (2016). Situating the default-mode network along a principal gradient of macroscale cortical organization. *Proceedings of the National Academy of Sciences, 113*, 12574–12579. doi:10.1073/pnas.1608282113

McKay, D. R., Knowles, E. E. M., Winkler, A. A. M., Sprooten, E., Kochunov, P., Olvera, R. L., … Glahn, D. C. (2014). Influence of age, sex and genetic factors on the human brain. *Brain Imaging and Behavior, 8*, 143–152. doi:10.1007/s11682-013-9277-5

Murphy, C., Wang, H.-T., Konu, D., Lowndes, R., Margulies, D. S., Jefferies, E., & Smallwood, J. (2019). Modes of operation: A topographic neural gradient supporting stimulus dependent and independent cognition. *NeuroImage, 186*, 487–496. doi:10.1016/j.neuroimage.2018.11.009

Palaniyappan, L. & Liddle, P.F. (2012). Differential effects of surface area, gyrification and cortical thickness on voxel based morphometric deficits in schizophrenia. *NeuroImage, 60*, 693–699. doi:10.1016/j.neuroimage.2011.12.058

Palaniyappan, L., Park, B., Balain, V., Dangi, R., & Liddle, P. (2015). Abnormalities in structural covariance of cortical gyrification in schizophrenia. *Brain Structure and Function, 220(4)*, 2059–2071. https://doi.org/10.1007/s00429-014-0772-2

Pasquier, F., Leys, D., Weerts, J. G., Mounier-Vehier, F., Barkhof, F., & Scheltens, P. (1996). Inter-and intraobserver reproducibility of cerebral atrophy assessment on MRI scans with hemispheric infarcts. *European Neurology, 36*, 268–272. doi:10.1159/000117270571

Pearl, J., & Bareinboim, E. (2014). External validity: From do-calculus to transportability across populations. *Statistical Science*, 579-595.

Rettmann, M. E., Kraut, M. A., Prince, J. L., & Resnick, S. M. (2006). Cross-sectional and longitudinal analyses of anatomical sulcal changes associated with aging. *Cerebral Cortex, 16(11)*, 1584–1594. doi:10.1093/cercor/bhj095

Roberts, M. A., & Caird, F. I. (1976). Computerised tomography and intellectual impairment in the elderly. *Journal of Neurology, Neurosurgery & Psychiatry, 39(10)*, 986–989. doi:10.1136/jnnp.39.10.986

Salat, D.H., Buckner, R.L., Snyder, A.Z., Greve, D.N., Desikan, R.S.R., Busa, E., Morris, J.C., Dale, A.M. & Fischl, B. (2004). Thinning of the cerebral cortex in aging. *Cerebral Cortex, 14*, 721–730. doi:10.1093/cercor/bhh032

Schaer, M., Cuadra, M. B., Tamarit, L., Lazeyras, F., Eliez, S., & Thiran, J.-P. (2008). A surface-based approach to quantify local cortical gyrification. *IEEE Transactions on Medical Imaging, 27(2)*, 161–170. doi:10.1109/tmi.2007.903576

Schaer, M., Cuadra, M.B., Schmansky, N., Fischl, B., Thiran, J.-P. & Eliez, S. (2012). How to measure cortical folding from MR images: A step-by-step tutorial to compute local gyrification index. *Journal of Visual Experiments, 59*, e3417. doi:10.3791/3417

Schaer, M., Ottet, M.-C., Scariati, E., Dukes, D., Franchini, M., Eliez, S., & Glaser, B. (2013). Decreased frontal gyrification correlates with altered connectivity in children with autism. *Frontiers in Human Neuroscience, 7*, 750. doi:10.3389/fnhum.2013.00750

Scheltens, P., Pasquier, F., Weerts, J. G., Barkhof, F., & Leys, D. (1997). Qualitative assessment of cerebral atrophy on MRI: Inter- and intra-observer reproducibility in dementia and normal aging. *European Neurology, 37*, 95–99. doi:10.1159/000117417

Shafee, R., Buckner, R. L., & Fischl, B. (2015). Gray matter myelination of 1555 human brains using partial volume corrected MRI images. *NeuroImage, 105*, 473–485. doi:10.1016/j.neuroimage.2014.10.054

Shen, X., Liu, T., Tao, D., Fan, Y., Zhang, J., Li, S., … Wen, W. (2018). Variation in longitudinal trajectories of cortical sulci in normal elderly. *NeuroImage, 166*, 1–9. doi:10.1016/j.neuroimage.2017.10.010

Sormaz, M., Murphy, C., Wang, H., Hymers, M., Karapanagiotidis, T., Poerio, G., Margulies, D. S., Jefferies, E., & Smallwood, J. (2018). Default mode network can support the level of detail in experience during active task states. *Proceedings of the National Academy of Sciences, 115*, 9318–9323. doi:10.1073/pnas.1721259115

Sowell, E.R., Peterson, B.S., Thompson, P.M., Welcome, S.E., Henkenius, A.L. & Toga, A.W. (2003) Mapping cortical change across the human life span. *Naure Neuroscience, 6*, 309–315. doi:10.1038/nn1008

Storsve, A. B., Fjell, A. M., Tamnes, C. K., Westlye, L. T., Overbye, K., Aasland, H. W., & Walhovd, K. B. (2014). Differential longitudinal changes in cortical thickness, surface area and volume across the adult life span: Regions of accelerating and decelerating change. *Journal of Neuroscience, 34(25)*, 8488–8498. doi:10.1523/jneurosci.0391-14.2014

Tomlinson, B., Blessed, G., & Roth, M. (1968). Observations on the brains of non-demented old people. Journal of the Neurological Sciences, 7, 331–356. doi:10.1016/0022-510x(68)90154-8

Turkheimer, E., Cullum, C. M., Hubler, D. W., Paver, S. W., Yeo, R. A., & Bigler, E. D. (1984). Quantifying cortical atrophy. *Journal of Neurology, Neurosurgery & Psychiatry, 47(12)*, 1314–1318. doi:10.1136/jnnp.47.12.1314

Yue, N. C., Arnold, A. M., Longstreth, W. T., Elster, A. D., Jungreis, C. A., O'Leary, D. H., ... Bryan, R. N. (1997). Sulcal, ventricular, and white matter changes at MR imaging in the aging brain: Data from the cardiovascular health study. *Radiology, 202*, 33–39. doi: 10.1148/radiology.202.1.8988189

Zilles, K., Armstrong, E., Schleicher, A., & Kretschmann, H.-J. (1988). The human pattern of gyrification in the cerebral cortex. *Anatomy and Embryology, 179*, 173-179. doi:10.1007/BF00304699

Appendix: Longitudinal changes in global cortical fractal dimensionality

Madan and Kensinger (2016) demonstrated that fractal dimensionality can be a more sensitive measure of age-related differences in cortical structure than conventional measures, including gyrification. To provide a complementary analysis here, although tangential to the focus of the current study, here I present the age-related longitudinal changes in fractal dimensionality, from the same data as included in the other analyses. To-date, longitudinal analyses of fractal dimensionality have not yet been conducted, and these results serve as an initial comparison between the gyrification results (e.g., participants in each panel are in the same line colour as in Figure 2). As expected from prior work, Figure A1 shows that there is less off-axis variability (i.e., random y-intercepts) with fractal dimensionality than are consistently found with gyrification. As with gyrification, a linear mixed effects model with random slopes for each participant was calculated, with a significant age fixed effect [$t(813)=25.55$, $p<.001$] with a decreasing slope of 0.01325 FD/decade [95% C.I. = 0.01223—0.01426].

As fractal dimensionality is a summary statistic of the complexity of a structure, a topographical analysis cannot be equivalently done as for gyrification—though fractal dimensionality can be calculated for parcellated cortical regions.

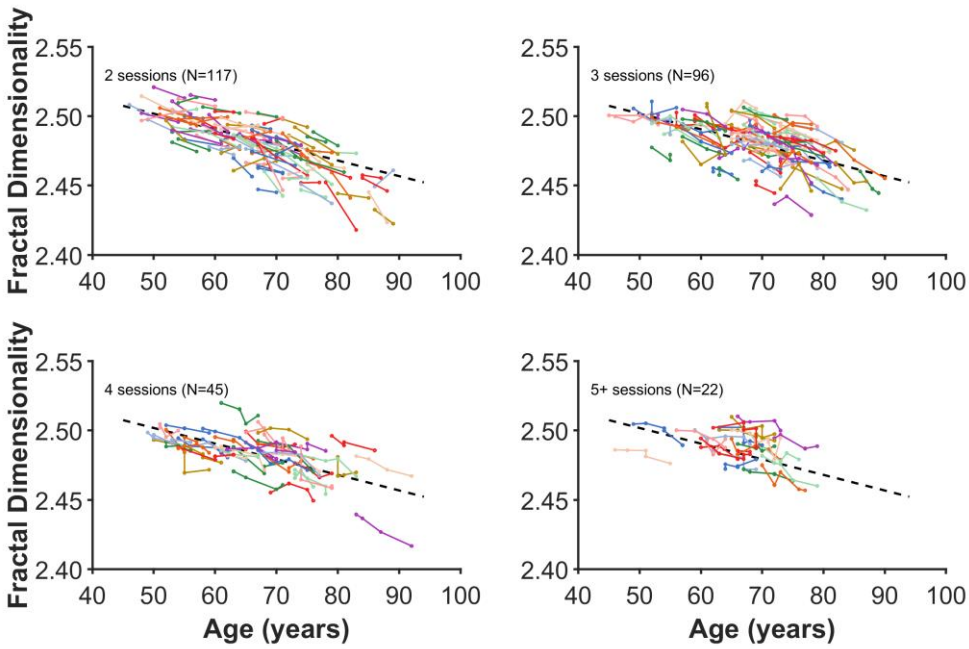

Figure A1. Age changes in global cortical fractal dimensionality. Each coloured line represents an individual participant, with each dot corresponding to an MRI session. The plot has been divided into panels for each set of timepoints to improve readability. Dashed line present in all panels shows the decrease in global gyrification based on all data, estimated using the linear mixed effects model. Compare with Figure 2.